Numerical and experimental analysis of the effect of forced cooling on laser tube forming

Khandandel, S. E., Seyedkashi, S. M. H. & Moradi, M.

Original citation & hyperlink:
Khandandel, SE, Seyedkashi, SMH & Moradi, M 2021, 'Numerical and experimental analysis of the effect of forced cooling on laser tube forming', Journal of the Brazilian Society of Mechanical Sciences and Engineering, vol. 43, no. 7, 338.
10.1007/s40430-021-03063-9

DOI 10.1007/s40430-021-03063-9
ISSN 1678-5878
ESSN 1806-3691

Publisher: Springer

The final publication is available at Springer via http://dx.doi.org/10.1007/s40430-021-03063-9

Numerical and experimental analysis of the effect of forced cooling on laser tube forming

S. Esmaeil Khandandel[1], S.M. Hossein Seyedkashi[1], Mahmoud Moradi[2*]

[1] *Department of Mechanical Engineering, University of Birjand, Birjand 97175-376, Iran*

[2] *School of Mechanical, Aerospace and Automotive Engineering, Faculty of Engineering, Environment and Computing, Coventry University, Coventry, United Kingdom*

Corresponding author email: ad6683@coventry.ac.uk

Abstract:

In the laser forming process, a cooling time is usually considered between successive scans to increase the temperature gradient and subsequently the bending angle. In this process, cooling is usually performed at ambient temperature, which can lead to a high increase in operation time and costs. The cooling rate can lead to undesirable changes in the microstructure depending on the type of material. In this research, by introducing a simple method for applying forced cooling with water at different distances from the laser beam, its effects are investigated on the laser forming of AISI 304L tubes using the finite element method and experiments. The bending angles and microstructure of the tube after forming is analyzed. The results show that local cooling with water reduces the duration of a 1-degree bend by about 8 to 13 times compared to the cooling at ambient temperature. However, local cooling with a small offset from the beam increases the residual stress after the forming, and consequently increases the probability of Stress Corrosion Cracking (SCC). However, cooling at ambient temperature increases the likelihood of intergranular precipitation in this steel compared to local cooling. According to the results, local cooling at a certain distance from the laser beam with the least change in residual stress has high efficiencies in bending the tube and less chance of corrosion after the forming.

Keywords: laser tube forming; cooling strategy; metallography; stress corrosion cracking; residual stress

1. Introduction

Laser tube forming (LTF) is a process in which the scanning of the tube surface by a defocused laser beam causes deformation. The power and diameter of this beam have to be adjusted so that no surface melting occurs during the scanning. There are two irradiation methods in LTF process; one in which the laser beam travels around the tube (circumferential scanning) and the other in which the laser beam travels along the tube axis (axial scanning). In axial scanning of the surface, the tube is fixed and the beam travels along the tube axis at a certain linear velocity and spot size. In circumferential scanning, the beam is fixed while the scan is performed by the rotational motion of the tube at a certain angular velocity.

More than two decades after the introduction of the LTF process, relatively a few studies have been conducted in this field. Therefore, the LTF process is still almost unknown compared to laser sheet forming [1]. This is due to the high complexity of this method and lack of economic interest to achieve a diverse and feasible deformation in comparison with conventional tube forming methods. In the research conducted by Li and Yao [2], the effective parameters in LTF have been studied numerically and experimentally. Hao and Li [3] presented an analytical model for calculating the bending angle to identify the relationship between the process parameters and the bending angle. Using the model proposed by Hao and Li [3], Imhan et al. [4] experimentally and analytically examined the changes in material properties during the laser forming. In another study, they also improved the bending angle in laser tube forming by increasing the absorption coefficient and formability of the material using laser softening heat treatment [5].

Circumferential and axial scanning were compared numerically and experimentally by Zhang et al. [6]. Safdar et al. [7] compared both methods under the same conditions. According to their results, the amount of bending in the axial scan was more favorable than in circumferential scanning. However, the bending angle in axial scanning is limited to the length of the tube. Also, re-scanning along the deformed tube is not possible due to change of defocused beam diameter. On the other hand, although the forming in circumferential scanning is more complex, multiple scanning is possible [2].

In general, both methods have their complexities and limitations in the implementation and achievement of the desired results which lie in the nature of laser forming. Research in laser forming shows that optimal deformation is dependent on several factors, including laser parameters, workpiece geometry, material properties, path strategy, and scanning method [8]. Keshtiara et al. [9] studied the multi-objective optimization of several process parameters using design of experiments techniques and genetic algorithm. However, the improvement and optimization of the results in tube forming requires extensive research on all of the mentioned parameters. It should be noted beforehand that to achieve a deformation with high accuracy and precision, it is necessary to keep the parameters constant in each forming.

In most studies, these parameters have been optimized under the shortening mechanism which researchers believe is the dominant mechanism [2, 3, 6, 7]. In the shortening mechanism, the tube diameter to beam diameter ratio is considered large for homogeneous heating in the thickness direction of the tube. Therefore, the scanned area is heated almost homogeneously. Increasing the temperature causes the material in the scanned area to expand, while the surrounding material resists this expansion. Therefore, the compressive plastic strain is created in the scanned areas, and as a result, after cooling down, the shortening in the direction of the tube axis causes the tube to bend toward the laser beam.

In recent years, effective steps have been taken for the 2D and 3D forming of tubes. Sheikholeslami et al. [10] reported that the bending angle of a square cross-section tube can be increased using a proper strategy in consecutive paths. The importance of path strategy in laser tube forming was highlighted in a study by Wang et al. [11]. In the mentioned research, a tube was three-dimensionally formed by designing a laser path strategy based on the combination of two 2D paths. Li et al. [12] succeeded in forming three-dimensional tubes by introducing a thread form path

strategy. Khandandel et al. [13] proposed a programmable design that could be used to form a wide range of 2D and 3D shapes on tubes.

However, achieving a certain bending angle in a successive scan requires allocating a cooling time between each scan; so, the processing time and cost increase. Therefore, Khandandel et al. [14] proposed a cooling strategy for reduction of the forming costs. The experiments performed in that research were in limited scope. Also, a theoretical and Numerical analyses of the effects of local cooling in LTF process could be of good progress in continuing of this study. In the present study, a forced cooling using water is proposed by local cooling at different distances from the laser beam center to reduce the final cost of multi-scanning laser forming. Also, its effect is investigated using experiments and Finite Element simulations on theoretical basis. Abaqus software is used to simulate this process to investigate the bending angles and residual stresses due to local cooling. The finite element model is validated by experiments. Finally, the microstructure of the material is studied to gain an overview of changes after the forming.

2. Materials and method

The LTF process was performed on a seamless and annealed tube made of AISI 304L stainless steel on a setup shown in Fig. 1. This tube was manufactured according to ASTM A 312/A 312M standard. Its chemical composition based on spectroscopic analysis is according to Table 1. The outer diameter of the tube is 12.25 mm with a thickness of 0.9 mm. The tube length is 90 mm, of which 30 mm is allocated for placement inside the chuck.

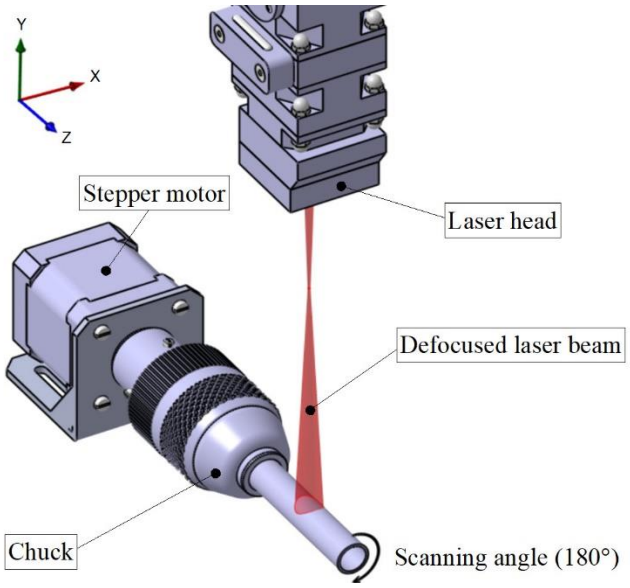

Fig. 1 Schematic of the circumferential scanning method

Table 1 Chemical composition of AISI 304L steel

Fe	C	Si	Mn	Cr	Ni	Mo	Cu	Co	Ti	Nb	V	N
<70.9	0.04	0.30	1.80	18.4	8.30	0.04	0.20	0.25	0.01	0.02	0.12	0.05

The laser path is set at a distance of 30 mm from the free edge of the tube. The laser beam is emitted from a fiber laser source with a maximum power of 1000 watts and a wavelength of 1080 nm. The scanning of the tube is performed in 2 seconds with an angular velocity of 90 degrees/sec, adjusted power of 668 watts, and the beam diameter of 10 mm. To achieve the desired bending angle, the scan is repeated for six times in a reciprocating manner. Also, the surface of the tube is covered with graphite spray after cleaning with propanol to increase the absorption coefficient of the beam. This can increase the laser absorption coefficient to about 60% [15].

The coupled temperature-displacement analysis is a good option for solving problems such as LTF where stress/strain depends on heat distribution analysis. The heat from plastic deformation is small and negligible compared to the heat input imposed by the laser. Therefore, heat-dependent properties such as thermal conductivity, specific heat, thermal expansion coefficient, modulus of elasticity, Poisson's ratio, and yield stress are defined in the model [16]. The material in the defined model is homogeneous and isotropic, and its density is constant during the process. Besides, the element type in this analysis should have degrees of freedom of temperature and stress. So, in this study, 16080 C3D8RT elements are used in simulations. This element is an 8-node thermally coupled brick with trilinear displacement and temperature, reduced integration, and hourglass control.

Since the heat required for laser forming is applied to the surface of the tube with a Gaussian distribution, the density of the heat flux caused by the laser scanning on the surface can be approximated by the following equation [17].

$$I = \frac{2AP}{\pi r_b^2} \exp(-\frac{2r^2}{r_b^2}) \quad (1)$$

where A is the absorption coefficient, P the output power of the laser, r_b the radius of the laser beam, and r the distance between the discussed point and the center of the laser beam. The amount and position of this heat flux versus time were developed and included in the Abaqus model using the DFLUX subroutine with the Fortran compiler.

Convection is modeled as forced heat convection for the surfaces in contact with water, and as natural (free) heat convection for other surfaces [18]. Convection follows Newton's law of cooling, and accordingly, the rate of heat loss due to convection is equal to Eq. (2) [19]:

$$q = h(T_s - T_E) \quad (2)$$

where the convective heat transfer coefficient h is a function of the temperature difference between the surface temperature T_s and the ambient temperature T_E and its value is defined by Eq. (3):

$$h = N_{ud}\left(\frac{k_f}{D}\right) \quad (3)$$

where N_{ud} is the Nusselt number, k_f the thermal conductivity of the fluid, and D the outer diameter of the tube.

For free heat convection, N_{ud} is calculated by the following equation [20]:

$$N_{ud}^{1/2} = 0.60 + 0.387\left(\frac{Gr_D Pr}{[1+(0.559/Pr)^{9/16}]^{16/9}}\right)^{1/6} \quad (4)$$

where Gr_D is the Grashof number and Pr the Prandtl number which is suitable for the range of $10^{-11} \leq Gr_D Pr \leq 10^9$.

Since the flow is perpendicular to the surface of the tube in the model designed for water cooling, N_{ud} for forced convection of heat transfer on the surfaces in contact with water is calculated by Eq. (5) [21]:

$$N_{ud} = 0.446{R_e}^{0.5}{P_r}^{0.35} + 0.528\left(\left(6.5e^{R_e/5000}\right)^{-5} + \left(0.031{R_e}^{0.8}\right)^{-5}\right)^{-1/5}{P_r}^{0.42} \quad (5)$$

where R_e is the Reynolds number which is valid in the range of $2 \times 10^3 < R_e < 10^5$ and $0.7 < P_r < 176$.

In both cases, the value of h at different temperatures is calculated and included in the model. Also, the rate of heat loss due to thermal radiation is equal to Eq. (6) [19]:

$$q = \sigma\varepsilon\left({T_s}^4 - {T_E}^4\right) \quad (6)$$

where σ is the called the Stefan–Boltzmann constant and ε is the emissivity.

As mentioned in the circular scanning of the tube for multiple scanning, a cooling time between each successive scan has to be considered in order to increase the temperature difference ΔT and achieve the maximum thermal strain ε_T according to Eq. (5).

$$\varepsilon_{T\,=}\, \alpha\Delta T \quad (7)$$

In the proposed cooling strategy, water is used as a coolant due to its high heat transfer coefficient. Therefore, cooling is faster and more efficient in reducing the cooling time and thus the production costs. On the other hand, heating and subsequent cooling can cause microstructural changes in the material. The type and amount of these changes are dependent on the temperature, heating duration, cooling method, and cooling rate. However, surface laser scanning in a thermal range below the melting temperature is a unique process that increases the temperature of the material in a short time and then rapidly cools down after irradiation. Therefore, there is not enough time to extensively change the microstructure of the material in this process. This will be discussed further in the following sections.

According to ASTM A 312/A 312M standard, in order to anneal the AISI 304L steel, its temperature must reach at least 1040 °C, and then it must be quenched in water. Therefore, an increase in the cooling rate is not a negative factor for this material.

This is important because the part cools rapidly after increasing the temperature due to beam scanning. This can cause extensive microstructural changes compared to non-scanned areas in the tube forming of especially carbon steels [22].

According to the proposed cooling strategy, water flows on the surface of the tube. As shown in Fig. 2a, two separators separate the laser-irradiated and water-cooled areas to prevent the reduction of laser efficiency. The distance (offset) between these two separators is defined in several levels to study the effects of different cooling rates.

Due to the relatively low thermal conductivity of AISI 304L [19], the offset size in this design is determined according to the full width at half maximum (FWHM) of the laser beam. Therefore, according to Eq. (8), FWHM for a beam diameter of 10 mm is about 6 mm [23].

$$FWHM = r_b\sqrt{2ln2} = 1.18r_b \quad (8)$$

The offset is defined in three levels of 7, 11, and 15 mm which are implemented according to Fig. 2. To determine the cooling time between each scan in Abaqus, the boundary conditions of each case were modeled for the three mentioned cases as well as the conditions in which the tube cools naturally. Based on the results of these simulations compared to the cooling at ambient temperature, the cooling rate increases with decreasing of the offset, and the heat dissipation is limited during the scan. The cooling rate and how the heat spreads in each design are shown in Fig. 3. Therefore, according to the results, the cooling time between each pass was allocated to achieve a minimum temperature of 35 degrees for each design. As a result, the parameters of the cooling designs are determined based on the simulation results and according to Table 2.

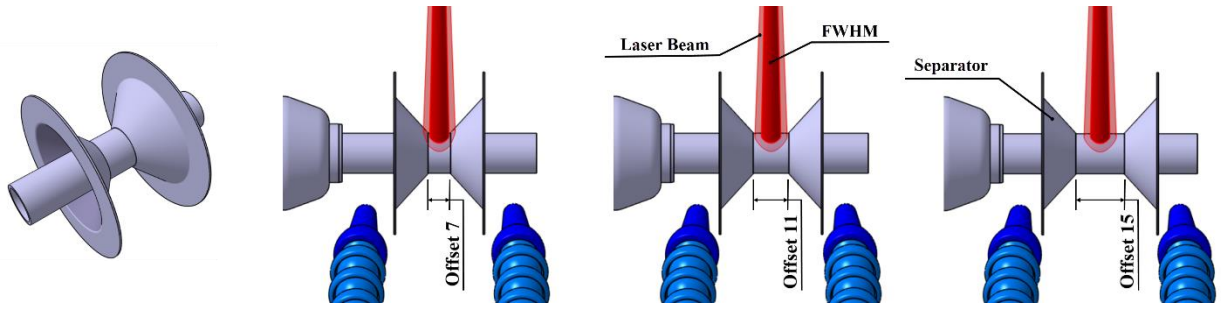

(a) (b) (c) (d)

Fig. 2 Offset position and location of separators in cooling designs a) positioning of separators around the irradiation zone, b) Offset 7mm, c) Offset 11mm, d) Offset 15mm

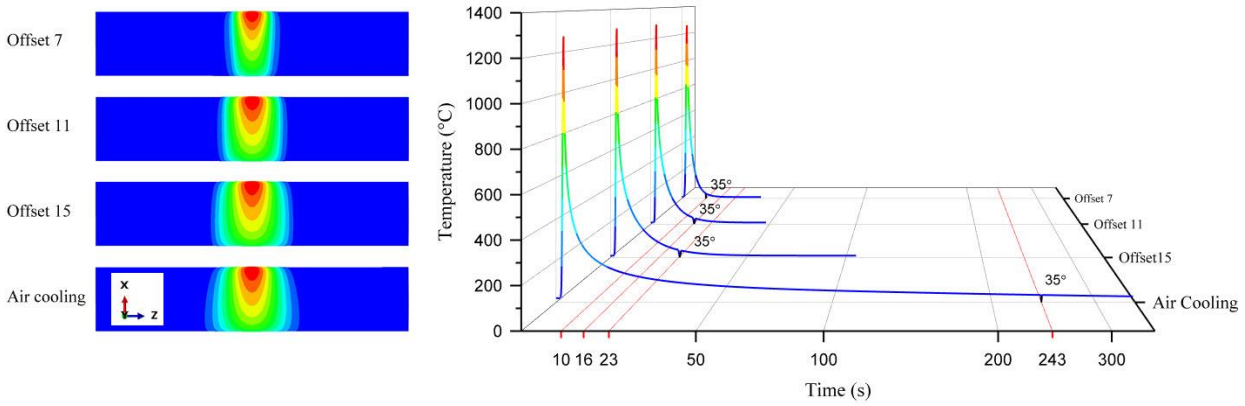

(a) (b)

Fig. 3 a) Comparison of temperature distribution based on the boundary conditions implemented in each design at the end of scanning, b) Comparison of heat growth and loss over time as a result of laser scan in each design

Table 2 The amount of cooling time between each scan

Cooling condition	**Cooling time (sec)**
Water cooling with offset 7 mm (design #1)	8
Water cooling with offset 11 mm (design #2)	14
Water cooling with offset 15 mm (design #3)	21
Natural cooling (design #4)	241

3. Results and discussion

Fig. 4 shows the bending angles obtained by experiments and FE simulations according to the proposed cooling designs. Three experiments were performed for each cooling design. The obtained results are in good agreement with each other. Fig. 5 shows that in design #1, part of the beam energy outside the offset range is absorbed by the separator. On the other hand, in this case, the water flow is at the closest distance to the center of heat, and heat transfer is more efficient than other cases, reducing the heat of these areas during scanning and subsequently increasing the cooling rate after scanning. Therefore, in the scanned areas in design #1, the heat and subsequent bending angles are less than in other cases. As shown in Fig. 4, with increasing the offset, the cooling effect during scanning is less.

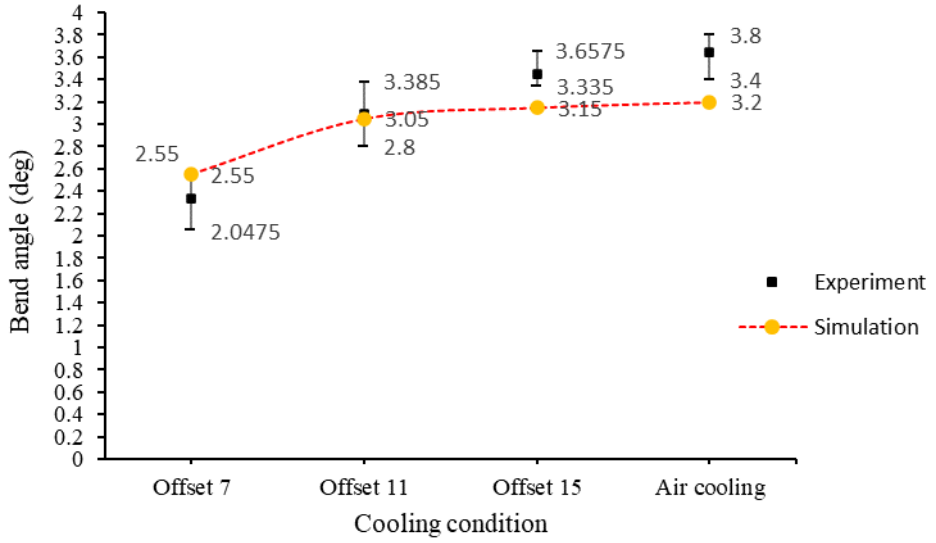

Fig. 4 Comparison of bending angles obtained from experiments and simulations

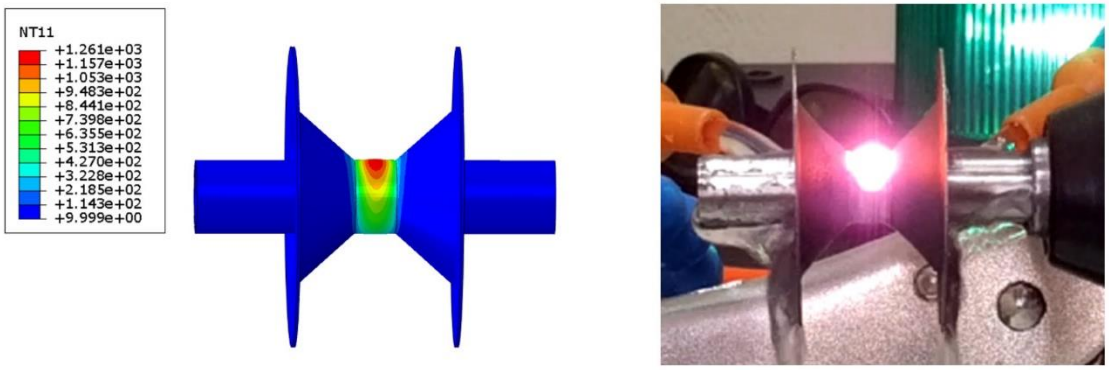

(a) (b)

Fig. 5 Heat distribution in design #1 (offset 7) at the end of scanning; a) Simulation, b) Experiment

As mentioned before, the shortening mechanism is the dominant mechanism in the laser tube forming process. At the beginning of the scan, the resistance of the areas around the scan zone against thermal strain causes a compressive elastic strain in the longitudinal and radial directions. At this time, due to the low thermal penetration depth along the thickness direction, the compressive elastic strain along the tube length is formed in the upper layer of the wall surface. Besides, the profile geometry and the tensile elastic strain toward the beam cause the scanned area to buckle toward the beam. At the beginning of the scan, the buckling occurs just in the elastic zone and is very small; however, its growth during the scan causes the formation of an arcuate bend after the end of the process. As shown in Fig. 6, as the scan continues in the specified path with the subsequent increase in temperature, the amount of compressive elastic strain along the tube length increases. Since increasing the temperature reduces the elastic modulus and yield

strength of the material in the central scanning area, the stress in this area exceeds the yield limit with the increase of the strain, and the compressive strain in the plastic area increases. As the scan continues, the heat becomes homogeneous along the entire wall thickness. Then, due to the volume constancy and the compressive strain applied to the central region, the material flows toward the center of irradiation and causes a bulge at the beam passage. The resulting shortening causes the tube to bend toward the beam.

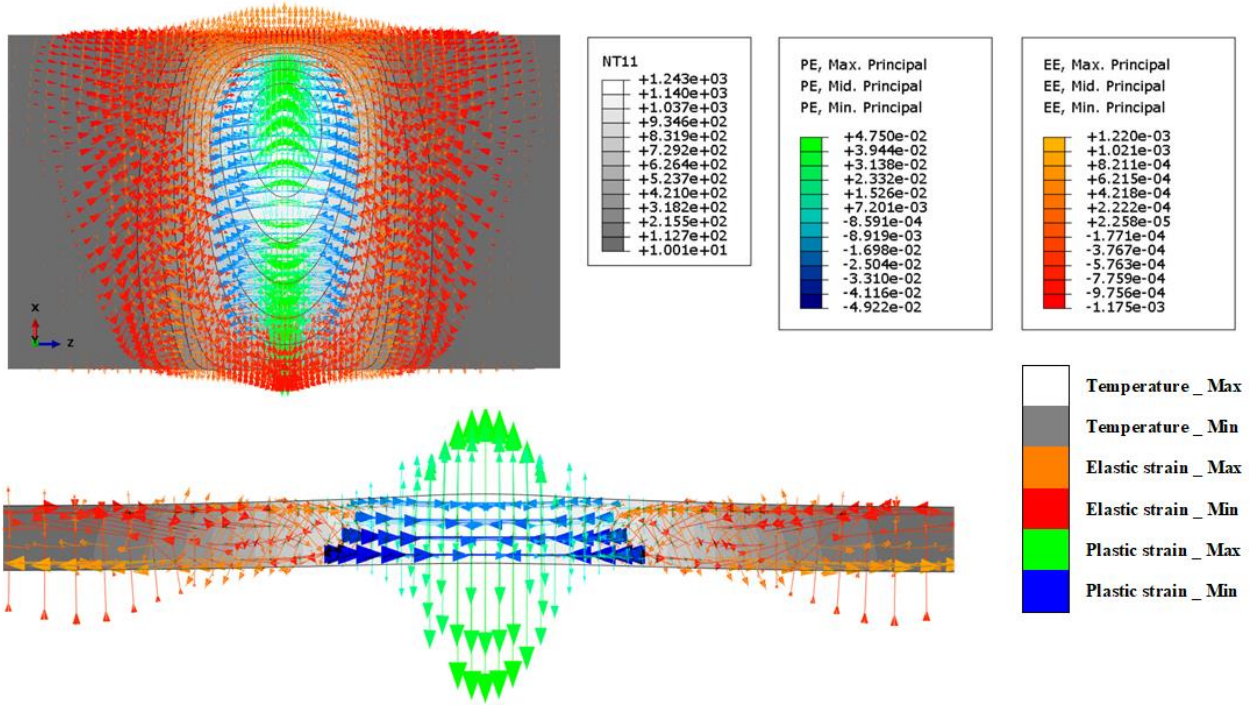

Fig. 6 Simultaneous display of the directions of main elastic and plastic strains and their relationship with the heat spread in the scanned area after 1.5 seconds from the first scan (Boundary conditions: design #1). As the temperature in the central scan area increases, the strain in the plastic area increases.

Fig. 7 compares the compressive plastic strain in the longitudinal direction of the tube in different designs, showing the increase in compressive strain in design #1 (offset 7mm). By increasing the offset, the obtained value gets closer to the natural cooling state. In this case, the heat does not increase as in the scanned areas because the areas around the beam are cooled with water. Consequently, the lack of considerable changes in the mechanical and thermal properties of the material around the scanned area causes a uniform resistance of materials in these areas against the thermal strain. Therefore, heat is trapped in the scanned area and increases the compressive plastic strain in the longitudinal direction of the tube. However, this increase in strain does not indicate the increase of bending angle. Fig. 7 shows that although the maximum compressive strain is higher in design #1, its amplitude is smaller than the other cases.

The cut section resulting from the forming according to design #1 in Fig. 7b shows that the tube has a small arcuate shape on the lower surface of the scanned area, and a bulged form on the

scanned surface. Also, by expanding the heat-affected zone (HAZ) in design #4, buckling plays a greater role in the shortening mechanism.

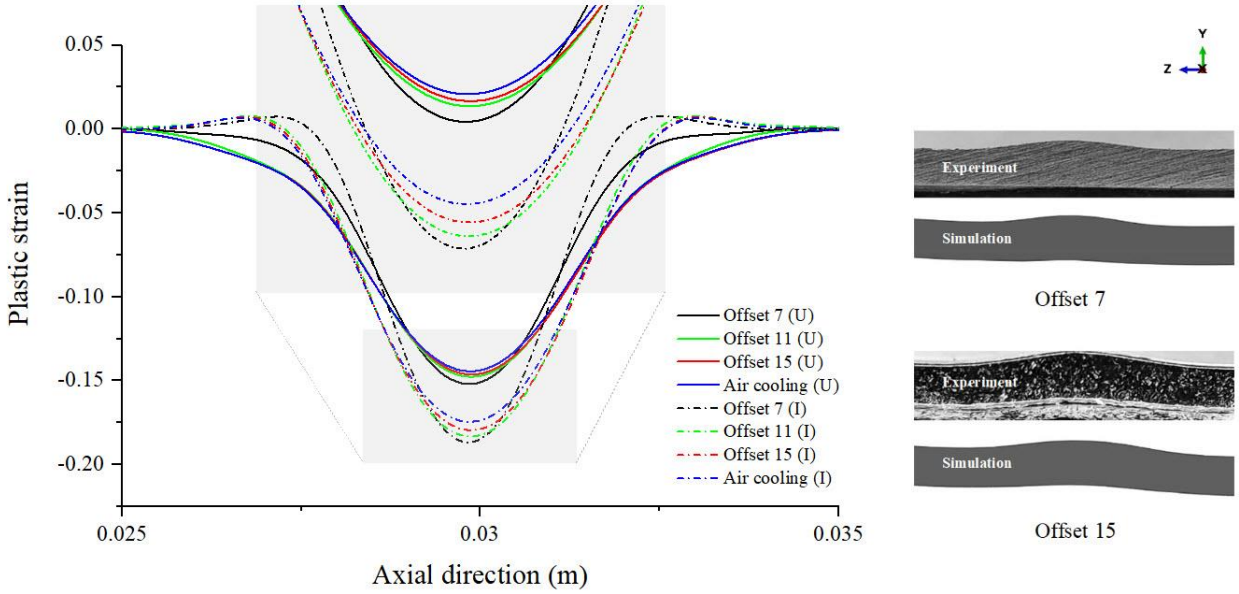

(a) (b)

Fig. 7 a) Comparison of axial plastic strain in different designs in the upper and lower layers of the scanned surface before the start of the second scanning, b) The effect of offset changes on the deformation of the scanned area in simulation and experiment after 6 scanning

As mentioned before, the concentrated resistance of the areas around the scan in design #1 has increased the compressive plastic strain. Investigation of residual stresses in different designs in Fig. 8 shows a considerable change in residual tensile stress in design #1 in the boundary area of cooling and laser scanning as a result of the concentrated reaction of the material to thermal strain after cooling. As the offset increases, the residual tensile stresses in design #2 are less than in design #1, and are least in designs #3 and #4. Because the presence of residual stresses of austenitic stainless steels in certain environments can lead to Stress Corrosion Cracking (SCC), the amounts of residual stress after forming is of particular importance and must be minimized [24].

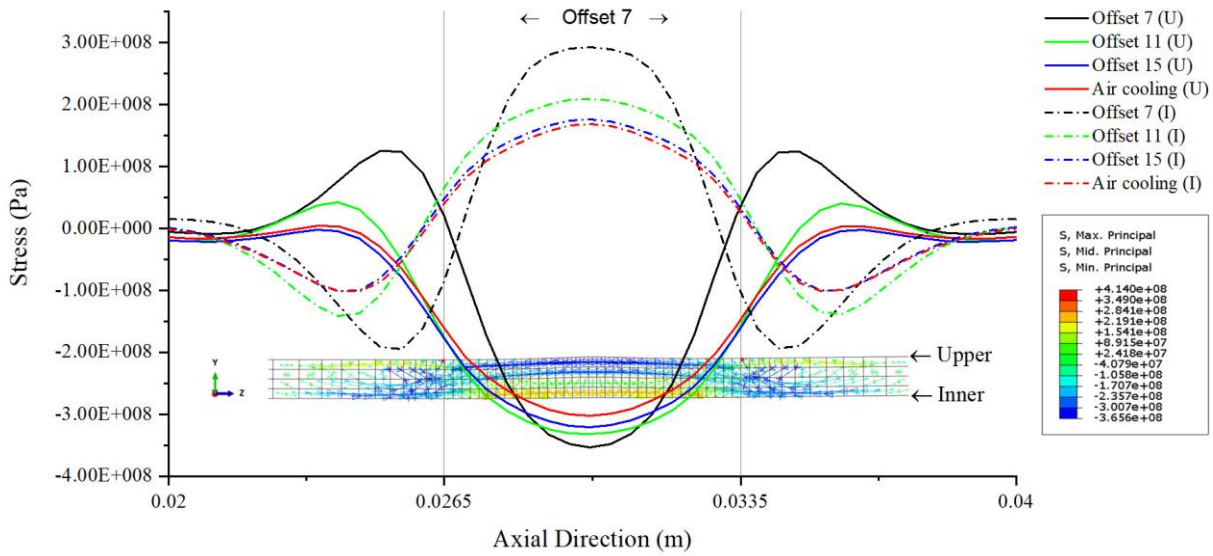

Fig. 8 Comparison of the axial stress in different designs in the upper and inner layers of the scanned surface before the second scanning. In the background, the main stress vectors of design #1 and their relationship to the maximum axial tensile stress are specified.

Comparison of the processing time in different designs in Table 3 shows that the processing time in water-cooled cases has been significantly reduced. A comparison of design #1 (offset 7mm) with design #4 (natural cooling) shows that the time required to bend one degree is about 13 times less than design #4. As a result, the cost is drastically reduced.

Table 3 Bending angles obtained with different cooling designs in experiments

Cooling design	Description	Cooling time (s)	Number of passes	Total time (s)	Average bending angle (°)	Bending angle (Degree / min)
#1	Water cooling with offset 7 mm	8	6	60	2.33	2.33
#2	Water cooling with offset 11 mm	14	6	96	3.09	1.93
#3	Water cooling with offset 15 mm	21	6	138	3.45	1.50
#4	Natural cooling	241	6	1217	3.65	0.18

AISI 304L stainless steel is a low carbon austenitic steel in an annealed state with an FCC structure. This group of steel is resistant to corrosion and oxidation, and is commonly used in humid or corrosive environments such as oil refineries and steam lines. Low carbon in this steel results in a reduction of carbide precipitation [25]. This category of steel is non-magnetic due to the austenitic structure in annealed condition [26]. The magnetic permeability of this steel is about 1.02 [27]. Therefore, structural changes that lead to a decrease in the percentage of austenite can increase the

magnetic permeability. Using the VSM device according to ASTM A342 / A342M standard, this value was measured as 1.010 for the reference sample at H=2000 Oe. The magnetic permeability of the cut sections of designs #1 to #4 is scattered in the range of 1.032 to 1.050. These values indicate slight changes in the percentage of austenite in the structure of the irradiated material after forming under all four conditions.

However, due to the dispersion of values and the number of samples, these values alone cannot be interpreted and relied upon. Therefore, the microstructures of material in different designs were also studied using a metallographic microscope.

According to the references [24, 25, 28] and the study of precipitation curves of $M_{23}C_6$ carbide as a common carbide in austenitic steels, the formation of precipitation is in the approximate temperature range 400 to 1000 °C, and the maximum precipitation rate is in the temperature range about 700 to 900 °C. The carbon and chromium dissolve in the austenite at temperatures above 1000 °C, and the precipitation rate decreases at temperatures below 500 °C and it is practically hard to form precipitations at these temperatures. However, the exposure time at these temperatures is an important factor of carbide precipitation, and the intergranular precipitation increases with increasing time. Therefore, after annealing of this group of steels at high temperatures, they have to be quenched in water to prevent carbide formation.

Chromium carbides precipitate at the grain boundaries due to their high energy [24]. Also, high-angle grain boundaries are good sites for chromium precipitation because of high atomic disorder where different orientations meet. On the other hand, the conditions for nucleation and growth of carbide particles at twin boundaries are not favorable [28].

Figs. 9b and 9c show minimal changes in the structure of the material in the scanned area in designs #1 and #2 compared to the parent structure (Fig. 9a). Also, the annealing twins seen in the reference sample can be detected in the irradiated areas in designs #1 and #2. As shown in Fig. 3, the rate of increase and decrease of heat in designs #1 and #2 is such that there is not enough opportunity for recrystallization and carbide precipitation. Hence, minimal changes have occurred in these cases. However, as mentioned earlier, residual stresses at the interface between separators and scanning areas can lead to SCC.

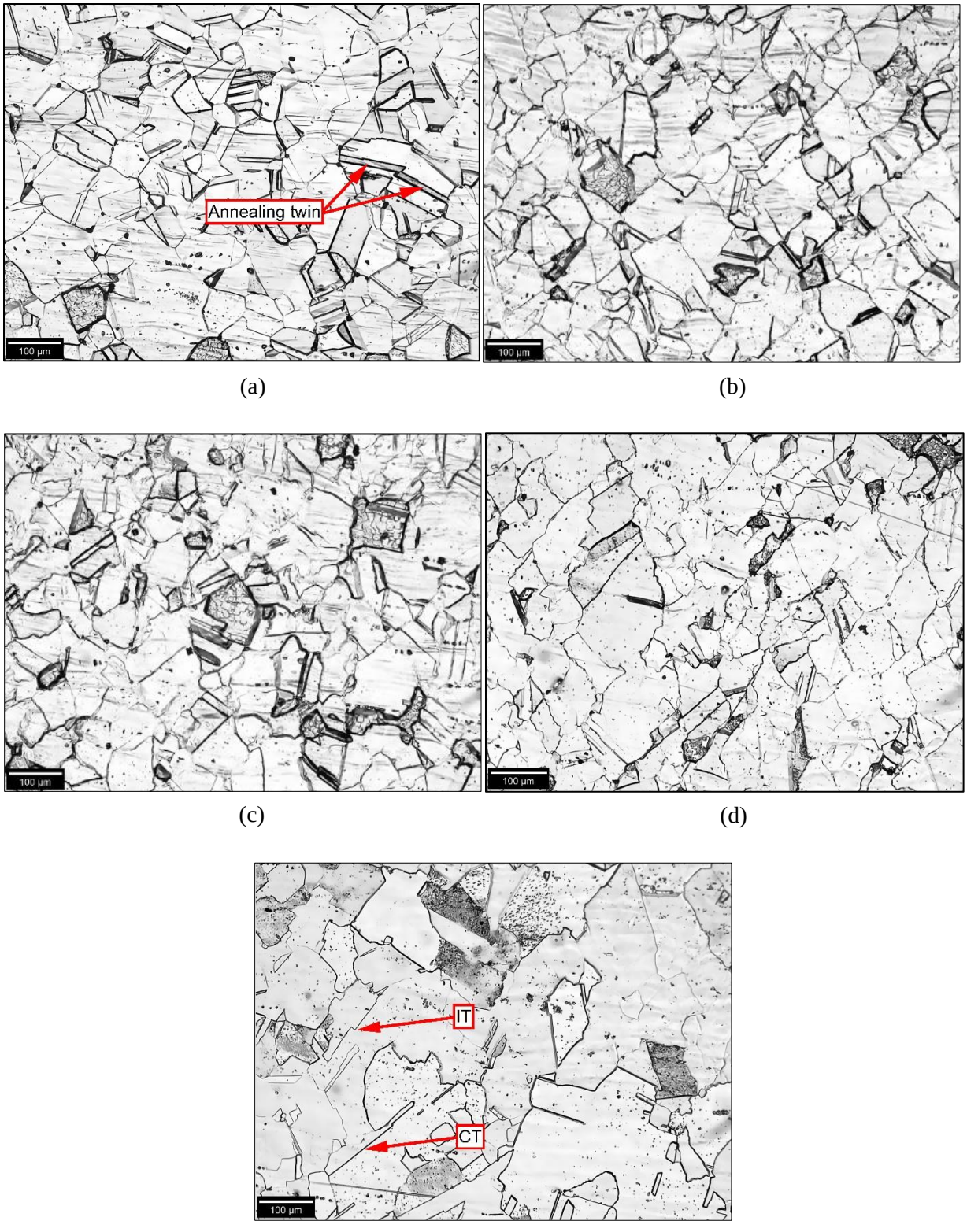

Fig. 9 Metallography of irradiated regions in; a) base material, b) Design #1, c) Design #2, d) Design #3, and e) Design #4 (Electrolyte: 10% oxalic acid)

Figs. 9d and 9e show a higher grain growth in design #4 than in design #3. As the cooling rate is reduced, there is an opportunity for recrystallization and grain growth. However, grain growth is more limited in design #3 and occurs in a narrow band in the central scanning zone. In design #4, the grain size is larger as well as its dispersion. Although the coherent plates in the microstructure of designs #3 and #4 weaken the carbide precipitation in these areas, increasing the grain size can increase the susceptibility of intergranular corrosion. Because the boundary area is larger in fine grains, there is less chance of forming a continuous carbide network in the grain boundaries [24]. However, there is more time for carbide precipitation in design #4 with natural cooling due to the large reduction of the cooling rate in comparison with design #3 (about 11 times less). The evidence indicates that the conditions for intergranular precipitation in design #4 are much more favorable than in other cooling designs. There is also a higher chance of SCC occurring in design #1 in certain environments. According to the results obtained from design #3, the probability of corrosion (both intergranular precipitation and SCC) in this design is less than in other cases. Also, the experiments showed that the offset tolerance has less effect on the final bending angle compared to designs #1 and #2. Therefore, the implementation of this plan (design #3) is simpler.

Finally, based on the obtained results, a tube has been successfully formed by the LTF process using six scans in nine consecutive paths according to design #3 (offset 15 mm). Fig. 10 shows the implementation of the sequential scanning according to this design. In this case, the total time spent on scanning and cooling between each pass for 54 scans is about 21 minutes. This time for the process with natural cooling (design #4) is about 3.5 hours.

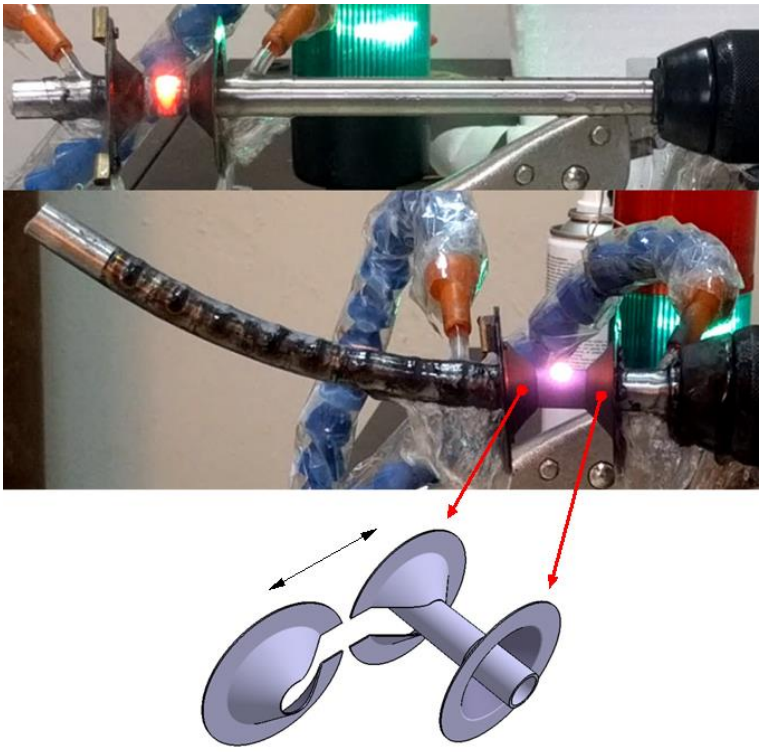

Fig. 10 Laser tube forming according to design #3 with 6 reciprocating scans in 9 consecutive identical paths

4. Conclusions

In this study, four cooling schemes were defined to investigate the effects of forced local cooling at different offsets (7, 11, 15 mm) from the beam in laser tube forming of AISI 304L. The process was experimentally investigated and also modeled using finite element simulation. It was concluded that:

1- The reduction of the cooling offset led to an increase in compressive plastic strain in the central irradiated area due to the increased concentration of resistance of surrounding materials against thermal strain.

2- The reduction of cooling offset increased the concentration of resistance to thermal strains in the areas around the scan which increased the residual stresses between the scanned and the surrounding areas. So, the minimum residual stress was obtained in the natural cooling design. The result of the cooling design with offset 15 mm was close to the natural cooling design. The reduction of cooling offset increases the probability of SCC formation in AISI 304L steel in certain environments due to the increase in residual stresses.

3- By reducing the offset and consequently increasing the cooling rate, the cooling time (delay) between each pass was reduced and as a result, the final cost of the process was drastically reduced compared to natural cooling. The processing time for creating a 1-degree bend with the cooling offset of 7 mm was about 13 times less than natural cooling.

4. In natural cooling, the slower cooling rate at ambient temperature in AISI 304L steel could increase the probability of intergranular deposition during the LTF process. This is due to the increase in the exposure time of materials to the temperature range of intergranular precipitation formation in this type of steel. However, the study of microstructures and magnetic permeability showed that intergranular precipitation was low due to the nature of the laser forming process and the mechanical properties of this steel.

5- With the largest offset (15 mm), the least probability of corrosion can be expected along with high efficiency of bending and the minimum residual stress. In this design, the effect of cooling offset from the center of the beam was minimized during scanning and only increased the cooling rate after scanning. Also, in this design, the offset position tolerance had less effect on the final bending angle than other designs.

Funding

This research did not receive any specific grant from funding agencies in the public, commercial, or not-for-profit sectors.

Declaration of competing interest

The authors declare that they have no known competing financial interests or personal relationships that could have appeared to influence the work reported in this paper.

References

[1] Guo Y, Shi Y, Wang X, Sun R, Li X (2021) A method to realize high-precision and large laser thermal bending angle. *J Manuf Process* 62:168–178. https://doi.org/10.1016/j.jmapro.2020.12.005

[2] Li W, Yao YL (2001) Laser Bending of Tubes: Mechanism, Analysis, and Prediction. *J Manuf Sci Eng* 123:674. https://doi.org/10.1115/1.1392992

[3] Hao N, Li L (2003) An analytical model for laser tube bending. *Appl Surf Sci* 208–209:432–436. https://doi.org/10.1016/S0169-4332(02)01428-9

[4] Imhan KI, Baharudin BTHT, Zakaria A, Ismail MISB, Alsabti NMH, Ahmad AK (2017) Investigation of material specifications changes during laser tube bending and its influence on the modification and optimization of analytical modeling. *Opt Laser Technol* 95:151–156. https://doi.org/10.1016/j.optlastec.2017.04.030

[5] Imhan KI, Baharudin BTHT, Zakaria A, Ismail MISB, Alsabti NMH, Ahmad AK (2018) Improve the material absorption of light and enhance the laser tube bending process utilizing laser softening heat treatment. *Opt Laser Technol* 99:15–18. https://doi.org/10.1016/j.optlastec.2017.09.040

[6] Zhang J, Cheng P, Zhang W, Graham M, Jones J, Jones M, Yao YL (2006) Effects of Scanning Schemes on Laser Tube Bending. *J Manuf Sci Eng* 128:20. https://doi.org/10.1115/1.2113047

[7] Safdar S, Li L, Sheikh MA (2007) Finite element simulation of laser tube bending: Effect of scanning schemes on bending angle, distortions and stress distribution. *Opt Laser Technol* 39:1101–1110. https://doi.org/10.1016/j.optlastec.2006.09.014

[8] Shi Y, Guo Y, Wang X, Sun R, Li X (2021) Laser bending angle and surface quality with preload at low heating temperature. *Opt Laser Technol* 136:106755. https://doi.org/10.1016/j.optlastec.2020.106755

[9] Keshtiara M, Golabi S, Tarkesh Esfahani R (2021) Multi-objective optimization of stainless steel 304 tube laser forming process using GA. *Eng Comput* 37:155–171. https://doi.org/10.1007/s00366-019-00814-0

[10] Sheikholeslami G, Griffiths J, Edwardson SP, Watkins K, Dearden G (2013) Laser Forming of ERW Steel Square Tubes within Metallurgical Constraints. In: K*ey Engineering Materials*. pp 68–75

[11] Wang XY, Luo YH, Wang J, Xu WJ, Guo DM (2013) Scanning path planning for laser bending of straight tube into coil-shape tube. *Int J Adv Manuf Technol* 69:909–917. https://doi.org/10.1007/s00170-013-5107-6

[12] Li F, Liu S, Shi A, Chu Q, Shi Q, Li Y (2019) Research on Laser Thread Form Bending of Stainless Steel Tube. *Int J Precis Eng Manuf* 20:893–903. https://doi.org/10.1007/s12541-019-00068-2

[13] Khandandel SE, Seyedkashi SMH, Moradi M (2020) Optik A novel path strategy design for precise 2D and 3D laser tube forming process ; experimental and numerical

investigation. *Opt - Int J Light Electron Opt* 206:164302. https://doi.org/10.1016/j.ijleo.2020.164302

[14] Khandandel SE, Seyedkashi SMH, Hoseinpour Gollo M (2020) Effect of Cooling on Bending Angle and Microstructure in Laser Tube Bending with Circumferential Scanning. *Iran J Mater Form* 7:14–23. https://doi.org/10.22099/IJMF.2019.34652.1137

[15] Cook F, Jacobsen V, Celentano D, Ramos-Grez J (2015) Characterization of the absorptance of laser irradiated steel sheets. *J Laser Appl* 27:032006. https://doi.org/10.2351/1.4918975

[16] Liu H (2013) Numerical analysis of thermal stress and deformation in multi-layer laser metal deposition processes. Masters Thesis, Missouri University of Science and Technology.

[17] Guan Y, Yuan G, Sun S, Zhao G (2012) Process simulation and optimization of laser tube bending. *Int J Adv Manuf Technol* 65:333–342. https://doi.org/10.1007/s00170-012-4172-6

[18] Boetcher SKS (2014) Natural convection from circular cylinders. Springer.

[19] Bergman TL, Lavine AS, Incropera FP, DeWitt DP (2017) Fundamentals of Heat and Mass Transfer. 8th ed, John Wiley & Sons.

[20] Churchill SW, Chu HHS (1975) Correlating equations for laminar and turbulent free convection from a horizontal cylinder. *Int J Heat Mass Transf* 18:1049–1053. https://doi.org/10.1016/0017-9310(75)90222-7

[21] Sanitjai S, Goldstein RJ (2004) Forced convection heat transfer from a circular cylinder in crossflow to air and liquids. *Int J Heat Mass Transf* 47:4795–4805. https://doi.org/10.1016/j.ijheatmasstransfer.2004.05.012

[22] Radek N, Kurp P, Pietraszek J (2019) Laser forming of steel tubes. *Czas Tech* 1:223–230. https://doi.org/10.4467/2353737xct.19.015.10055

[23] Rolt S (2020) Optical Engineering Science. John Wiley & Sons. https://doi.org/10.1002/9781119302773

[24] Khatak HS, Raj B (2002) Corrosion of austenitic stainless steels: mechanism, mitigation and monitoring. Woodhead publishing

[25] Cramer SD, Covino BS (2018) Corrosion: Fundamentals, Testing, and Protection. ASM International

[26] Graham CD, Lorenz BE (2018) Delta ferrite is ubiquitous in type 304 stainless steel: Consequences for magnetic characterization. *J Magn Magn Mater* 458:15–18. https://doi.org/10.1016/j.jmmm.2018.02.092

[27] Moosbrugger C (2000) ASM ready reference Electrical and magnetic properties of metals. ASM International

[28] Krauss G (2015) Steels: Processing, Structure, and Performance, Second Edition - ASM International